The Astrophysical Journal, 943:38 (15pp), 2023 January 20 https://doi.org/10.3847/1538-4357/aca662


# Statistics of Galactic-scale Quasar Pairs at Cosmic Noon

Yue Shen[1,2], Hsiang-Chih Hwang[3], Masamune Oguri[4,5], Nianyi Chen[6], Tiziana Di Matteo[6,7], Yueying Ni[6,7], Simeon Bird[8], Nadia Zakamska[3,9], Xin Liu[1,2], Yu-Ching Chen[1], and Kaitlin M. Kratter[10]
[1] Department of Astronomy, University of Illinois at Urbana-Champaign, Urbana, IL 61801, USA; shenyue@illinois.edu
[2] National Center for Supercomputing Applications, University of Illinois at Urbana-Champaign, Urbana, IL 61801, USA
[3] School of Natural Sciences, Institute for Advanced Study, 1 Einstein Drive, Princeton, NJ 08540, USA
[4] Center for Frontier Science, Chiba University, 1-33 Yayoi-cho, Inage-ku, Chiba 263-8522, Japan
[5] Department of Physics, Graduate School of Science, Chiba University, 1-33 Yayoi-Cho, Inage-Ku, Chiba 263-8522, Japan
[6] McWilliams Center for Cosmology, Department of Physics, Carnegie Mellon University, Pittsburgh, PA 15213, USA
[7] NSF AI Planning Institute for Physics of the Future, Carnegie Mellon University, Pittsburgh, PA 15213, USA
[8] Department of Physics & Astronomy, University of California, Riverside, 900 University Avenue, Riverside, CA 92521, USA
[9] Department of Physics and Astronomy, Johns Hopkins University, Baltimore, MD, USA
[10] University of Arizona, 933 North Cherry Avenue, Tucson, AZ 85721, USA
*Received 2022 August 11; revised 2022 November 2; accepted 2022 November 11; published 2023 January 23*

## Abstract

The statistics of galactic-scale quasar pairs can elucidate our understanding of the dynamical evolution of supermassive black hole (SMBH) pairs, the duty cycles of quasar activity in mergers, or even the nature of dark matter, but they have been challenging to measure at cosmic noon, the prime epoch of massive galaxy and SMBH formation. Here we measure a double quasar fraction of $\sim 6.2 \pm 0.5 \times 10^{-4}$ integrated over $\sim 0\farcs3$–$3''$ separations (projected physical separations of $\sim$3–30 kpc at $z \sim 2$) in luminous ($L_{\rm bol} > 10^{45.8}$ erg s$^{-1}$) unobscured quasars at $1.5 < z < 3.5$ using Gaia EDR3-resolved pairs around SDSS DR16 quasars. The measurement was based on a sample of 60 Gaia-resolved double quasars (out of 487 Gaia pairs dominated by quasar+star superpositions) at these separations, corrected for pair completeness in Gaia, which we quantify as functions of pair separation, magnitude of the primary, and magnitude contrast. The double quasar fraction increases toward smaller separations by a factor of $\sim$5 over these scales. The division between physical quasar pairs and lensed quasars in our sample is currently unknown, requiring dedicated follow-up observations (in particular, deep, subarcsecond-resolution IR imaging for the closest pairs). Intriguingly, at this point, the observed pair statistics are in rough agreement with theoretical predictions both for the lensed quasar population in mock catalogs and for dual quasars in cosmological hydrodynamic simulations. Upcoming wide-field imaging/spectroscopic space missions such as Euclid, CSST, and Roman, combined with targeted follow-up observations, will conclusively measure the abundances and host galaxy properties of galactic-scale quasar pairs, offset AGNs, and subarcsecond lensed quasars across cosmic time.

*Unified Astronomy Thesaurus concepts:* Black hole physics (159); Active galaxies (17); Double quasars (406)

*Supporting material:* machine-readable tables

## 1. Introduction

The formation of binary supermassive black holes (SMBHs; $M_{\rm BH} \gtrsim 10^6\,M_\odot$) is the inevitable consequence of galaxy mergers and the prevalence of SMBHs in galactic nuclei (e.g., Begelman et al. 1980). After the merger of two galaxies, the two SMBHs will inspiral in the merged galaxy due to dynamical friction from tens of kiloparsecs to $\sim$10 pc (e.g., Milosavljević & Merritt 2001; Yu 2002; Merritt 2013). The two SMBHs become a gravitationally bound binary at $\lesssim$10 pc separations, and interactions with stars continue to shrink the binary orbit. The evolution of the binary SMBH below $\sim$1 pc depends on the properties of stellar orbits in the galactic potential and the effects of gas (e.g., Merritt 2013; De Rosa et al. 2019). But if the binary orbit can shrink to scales $\ll$1 pc, gravitational-wave (GW) radiation will take over in shrinking the binary orbit and eventually lead to the coalescence of the two SMBHs. The GW signals during the final inspiral and coalescence of the binary SMBH are highly anticipated from ongoing pulsar timing arrays (e.g., Arzoumanian et al. 2020) and future GW facilities such as the Laser Interferometer Space Antenna (e.g., Amaro-Seoane et al. 2022).

The SMBH pairs at galactic-scale separations (tens of kiloparsecs to tens of parsecs) represent the best-understood stage in theoretical studies of binary SMBH formation. The abundance of these wide-separation pairs sets the initial conditions of binary SMBHs expected from galaxy mergers. Their pair separation statistics constrain the evolutionary timescales of galactic-scale SMBH pairs, which can be compared with analytical calculations or numerical simulations (e.g.,Merritt 2013; De Rosa et al. 2019, and references therein). Dynamical friction dominates the orbital evolution of these pairs before they become bound binaries. Nevertheless, there are still lingering theoretical uncertainties in this regime, and the timescale spent at these galactic-scale separations depends on the galaxy potential, mass ratio of the merging galaxies, and properties of the stellar cores surrounding each SMBH, as well as the effects of gas (both dynamical and accretion onto SMBHs) and dark matter halo properties (e.g., Milosavljević & Merritt 2001; Yu 2002; Callegari et al. 2009, 2011; Khan et al. 2013; McWilliams et al. 2014; Kelley et al. 2017; Tamfal et al. 2018; Tremmel et al. 2018; Xiao et al. 2021; Chen et al. 2022a).

Observationally, galactic-scale SMBH pairs can be identified as dual active galactic nuclei (AGNs) or luminous dual quasars (conventionally defined by $L_{\rm bol} \gtrsim 10^{45}$ erg s$^{-1}$) if both SMBHs are active. Inactive SMBH pairs on galactic scales are difficult to identify at cosmological distances. Pairs with only one active SMBH may appear as an offset AGN (e.g., Barrows et al. 2016). But the detection of offset AGNs becomes challenging at $z > 1$, requiring deep, high-resolution imaging/spectroscopy and robust measurements of the host galaxy centroid, as well as careful treatments of selection effects (e.g., Stemo et al. 2021). Alternatively, it is possible to use high-resolution ALMA observations to measure the host galaxy at $z \gtrsim 6$ and reveal a potential offset AGN (e.g., Venemans et al. 2020).

These dual AGNs/quasars signpost galactic-scale SMBH pairs and can be used to constrain the underlying SMBH pair population if the AGN duty cycle can be reliably inferred from hydrodynamic simulations. With sufficient statistics to explore the diversity of the SMBH pair population, such as host galaxy properties and redshift evolution, observations of these pairs will enable critical comparisons with theoretical models.

The pairing and dynamical evolution of SMBHs at $z \sim 2$ is of particular importance. The specific galaxy merger rate is much higher at cosmic noon than at lower redshifts (e.g., Duncan et al. 2019), where both luminous quasars and global star formation reached their peak activity around $z \sim 2$ (e.g., Richards et al. 2006; Madau & Dickinson 2014). This is the prime epoch of the growth of massive SMBHs and galaxies and the onset of formation of the most massive (e.g., $>10^8\,M_\odot$) SMBH binaries, whose eventual coalescence will dominate the GW signal in the pulsar timing array band. The statistics of galactic-scale SMBH pairs at cosmic noon, as traced by dual quasars, provide critical constraints on the dynamical friction timescales, as well as the impact of galaxy mergers on the fueling of SMBHs.

The pair statistics down to ∼1 kpc may even constrain the nature of dark matter. For example, in the fuzzy dark matter (FDM) model (Hu et al. 2000) and neglecting baryonic effects, SMBH pairs would never get much closer than ∼1 kpc because FDM fluctuations inhibit the orbital decay and inspiral at ∼kiloparsec scales (Hui et al. 2017), resulting in a "pileup" of SMBH pairs at ∼1 kpc. A spike in the dual quasar fraction toward ∼1 kpc, above the level that can be explained by quasar duty cycle enhancement in mergers, may be the smoking gun signature of FDM.

Unfortunately, given the stringent spatial resolution requirement (e.g., subarcseconds for ∼kiloparsec scales) and the apparent rareness of such pairs, the observational inventory of $z > 1.5$ dual quasars at ≲tens of kiloparsec separations remains scarce. There are only a handful of serendipitously discovered ∼kiloparsec-scale dual/offset AGNs known at lower redshifts (e.g., Komossa et al. 2003; Comerford et al. 2009; Civano et al.2010; Liu et al. 2010; Goulding et al. 2019). Dedicated wide-area searches of binary quasars[11] at $z > 1.5$ have compiled tens of quasar pairs at projected separations of $10\,{\rm kpc} \lesssim r_p \lesssim 50\,{\rm kpc}$ (e.g., Hennawi et al. 2006; Myers et al. 2008; Hennawi et al. 2010; Kayo & Oguri 2012; More et al. 2016; Eftekharzadeh et al. 2017), starting to probe the galactic-scale environment of quasar pairs. But the $r_p < 10$ kpc regime of high-redshift quasar pairs remains largely unexplored (Figure 1 in Chen et al. 2022d) due to the lack of efficient quasar identification for subarcsecond pairs that are typically unresolved in ground-based data. Assuming no merger-enhanced AGN duty cycles and applying the dynamical friction prediction of galactic-inspiral timescales (i.e., the dynamical friction timescale $t_{\rm df}$ is roughly proportional to $r$, the 3D pair separation; e.g., Yu 2002; Chen et al. 2020), we expect an ∼kiloparsec-scale dual quasar fraction of $f_{\rm QQ} \sim 5 \times 10^{-5}$ among all quasars, extrapolated from the observed quasar pair statistics on tens of kiloparsec scales (e.g., $f_{\rm QQ} \sim 5 \times 10^{-4}$; Kayo & Oguri 2012). To test these expectations, we need to search a large parent quasar sample in order to build up the statistics of rare dual quasars.

In this work, we measure the galactic-scale (i.e., $r_p \lesssim 30$ kpc) quasar pair fraction at $z \sim 2$ using a different approach than earlier studies (e.g., Hennawi et al. 2006; Myers et al. 2008; Hennawi et al. 2010; Kayo & Oguri 2012; More et al. 2016; Eftekharzadeh et al. 2017; Silverman et al. 2020), focusing on the $r_p < 10$ kpc regime that has been poorly explored before. Our approach builds on the all-sky Gaia survey Early Data Release 3 (EDR3; Fabricius et al. 2021), which provides precise coordinates, magnitudes, and astrometric measurements for all-sky sources to as faint as $G \sim 21$. In particular, Gaia's nominal ∼0.″2 resolution enables the identification of close-separation companions around distant quasars, with quantifiable completeness in resolved pairs as a function of angular separation (Section 2). Importantly, Gaia proper-motion measurements enable efficient separation of stars and quasars, a unique advantage that previous quasar pair searches based on photometric color selection did not have. There is no need to update our analysis using the recent Gaia DR3 release (Gaia Collaboration et al. 2022), since the photometric and astrometric content is essentially unchanged from EDR3 to DR3.

This paper is organized as follows. In Section 2, we describe the sample and data used in our systematic search of high-redshift small-scale quasar pairs, with an emphasis on quantifying the completeness of Gaia EDR3-resolved pairs. We present our results in Section 3, where we compare the observed pair statistics with theoretical predictions of lensed quasars and quasar pairs. We discuss the implications of our findings in Section 4 and summarize in Section 5. In this work, we focus on luminous unobscured broad-line quasars exclusively, given the survey depth of Gaia. Occasionally, we use the term "dual quasars" to refer to physical quasar pairs on galactic scales, following the convention for dual AGNs at $z < 1$ (e.g., Comerford et al. 2009) that have much lower luminosities than our quasars. By default, quasar pairs refer to physically associated pairs within the merging galaxies, rather than unrelated, projected quasar pairs at different redshifts. For practical purposes, we use the term "double quasars" to collectively refer to quasar pairs and lensed quasars. We adopt a flat ΛCDM cosmology with $\Omega_\Lambda = 0.7$, $\Omega_M = 0.3$, and $H_0 = 70\,{\rm km\,s^{-1}\,Mpc^{-1}}$. Pair physical separations are measured in proper units.

## 2. Data

We start from the latest compilation of spectroscopically confirmed quasars in the Sloan Digital Sky Survey (SDSS) DR16 (DR16Q; Lyke et al. 2020) and restrict our search to $z > 1.5$ quasars. This redshift cut is crucial to this study and ensures negligible emission from the host galaxy within the Gaia bandpass, which would complicate the source detection and

[11] For historical reasons, these wide-separation pairs are referred to as "binary quasars" (e.g., Djorgovski 1991; Kochanek et al. 1999), as the two SMBH +galaxy systems are bound to each other.

astrometry measurements (Hwang et al. 2020). We then search for Gaia EDR3 sources in a 3″ radius circular region around each SDSS quasar. We further require the matched Gaia sources to have $G < 20.25$, which balances the needs for pair statistics and high completeness in Gaia detection and astrometric measurements. For example, Fabricius et al. (2021) demonstrated nearly 100% completeness of photometric detection at $G = 20$ in low stellar density fields with Gaia EDR3, applicable to SDSS quasars. We have tested Gaia's photometric detection completeness for single sources using the DR16Q quasar catalog and find that the completeness is $\sim 98.12\% \pm 0.41\%$ even in the faintest bin, $G = [20, 20.25]$.

Our $G < 20.25$ flux limit roughly corresponds to bolometric luminosity $L_{\rm bol} > 10^{45.8}$ erg s$^{-1}$ at $z > 1.5$ (Shen et al. 2011), or SDSS $i < 20.13$ (we adopt a magnitude conversion of $G = i + 0.12$ assuming a fixed quasar power-law continuum $f_\nu \propto \nu^{-0.5}$). The parent sample satisfying these redshift and magnitude cuts and having single Gaia matches includes 134,796 DR16Q quasars.

We focus on Gaia-resolved double sources at the SDSS quasar position. Multiple systems with more than two Gaia sources brighter than $G = 20.25$ within 3″ are only ∼2% of double systems and hence negligible. A more important issue is that the completeness of these multiples is much lower and harder to quantify; thus, we ignore this higher-order multiple population. Some quasars with only one matched Gaia source may still be a subarcsecond quasar pair, which can be recovered with other approaches using additional Gaia parameters (e.g., Shen et al. 2019; Hwang et al. 2020; Chen et al. 2022d; Makarov & Secrest 2022; Mannucci et al. 2022), but are not covered here; instead, their contribution to the pair statistics is estimated through the completeness analysis (Section 2.3).

**Table 1**
Pair Sample Data

| Column (1) | Format (2) | Units (3) | Description (4) |
|---|---|---|---|
| SDSS_NAME | STRING | | J2000 hhmmss.ss ± ddmmss.s |
| Z | DOUBLE | | Default redshift from DR16Q |
| PLATE | LONG | | Plate number (SDSS spec) |
| FIBERID | LONG | | FiberID (SDSS spec) |
| MJD | LONG | | MJD (SDSS spec) |
| GAIA_RA1 | DOUBLE | deg | Gaia RA |
| GAIA_DEC1 | DOUBLE | deg | Gaia DEC |
| GAIA_RA2 | DOUBLE | deg | Gaia RA |
| GAIA_DEC2 | DOUBLE | deg | Gaia DEC |
| G1 | DOUBLE | mag | Gaia G mag |
| G2 | DOUBLE | mag | Gaia G mag |
| BP_RP1 | DOUBLE | mag | Gaia BP-RP color |
| BP_RP2 | DOUBLE | mag | Gaia BP-RP color |
| PM_SIG1 | DOUBLE | | PM significance |
| PM_SIG2 | DOUBLE | | PM significance |
| PAIR_SEP | DOUBLE | arcsec | Pair separation |
| TYPE | STRING | | Pair classification |
| KNOWN | STRING | | Literature classification |
| F_COMP | DOUBLE | | Pair completeness (Section 2.3) |

**Note.** For each pair, index 1 refers to the DR16Q quasar and 2 refers to the companion, regardless of their relative brightness (i.e., the quasar can be fainter than the companion, especially at large pair separations). Gaia measurements are from EDR3 (null values are "NaN"). The column "TYPE" indicates pair classification: "QQ" refers to a double quasar, "QS_PM" refers to a quasar +star pair based on proper motion, and "QS_PCA" refers to a quasar+star pair based on spectral PCA; one quasar (J0033+2015) is a known quasar+star pair (More et al. 2016), and we set its TYPE = "QS_KNOWN." The associated FITS file is available in the online version of this paper.

(This table is available in its entirety in machine-readable form.)

### 2.1. The Pair Sample

Our initial Gaia-resolved pair sample includes 497 SDSS DR16Q quasars. However, in 10 pairs, both components are bona fide quasars listed in DR16Q and thus are counted twice. Removing these 10 duplicated pairs, our final Gaia-resolved pair sample includes 487 unique pairs. For each pair, the closer Gaia match is designated as the corresponding SDSS DR16Q quasar. This is generally the case. However, in very rare cases of pairs separated by $\lesssim 1''$, the SDSS optical centroid may be dominated by the companion. Nevertheless, this detail does not affect any of our statistical analyses below. We classify the companion as "starlike" in 416 pairs where its proper motion is detected by Gaia at $>3\sigma$ significance; for comparison, only ∼2% of Gaia singly matched quasars have $>3\sigma$ proper-motion detection, meaning that our proper-motion cut will only inadvertently exclude a negligible fraction of bona fide double quasars. The remaining 71 resolved pairs are our initial sample of double quasars. Pair separations are computed using Gaia EDR3 coordinates, which can slightly exceed the 3″ cross-matching radius between SDSS and Gaia. The full pair catalog of 487 pairs is presented in Table 1.

Figure 1 (left) shows the distributions of Gaia BP − RP color for the DR16Q quasar in the pair and the starlike and "quasar-like" companions for the full Gaia pair sample. Because Gaia photometry is measured within a $3\farcs5 \times 2\farcs1$ window (Riello et al. 2021), source deblending may be significantly impacted for the closest pairs. Thus, we have excluded pairs with separations $<1''$ in this color distribution plot to avoid cross talk in their photometric color measurements. Their color distributions suggest that starlike companions indeed have different colors than the primary quasars or the quasar-like companions based on Gaia proper-motion detection.

Figure 1 (right) shows the distributions of pair separation for double systems with starlike and quasar-like companions. The separation distribution for starlike companions rapidly declines toward smaller separations, as anticipated from the reduction of the geometric cross section and the constant sky density of a foreground (star) population, modulo pair-resolving incompleteness toward $\lesssim 1''$ separations. In contrast, the separation distribution for quasar-like companions remains more or less constant, suggesting that it is an intrinsic population associated with the primary quasar. Both the color and separation distributions in Figure 1 indicate that the classification of star and quasar companions based on proper motion is reasonably good, given the markedly different distributions for the two populations. Of course, it is possible that some detected proper motions are caused by systematics (especially for subarcsecond pairs where the two sources overlap in photometric/astrometric measurements). Here we opt to exclude these potential double quasars misidentified as quasar+star pairs due to potentially compromised proper-motion measurements due to close neighbors, in order to maintain a high-purity double quasar sample. Figure 2 displays additional statistical properties of the parent pair sample.

Likewise, we expect that there is still residual contamination of star superposition in these close pairs that we classified as

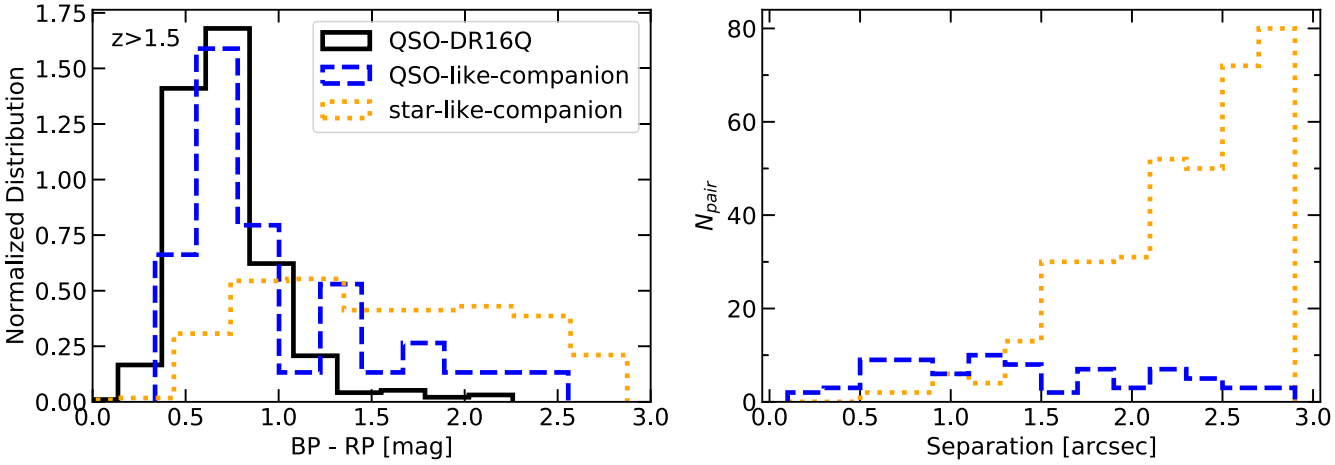


**Figure 1.** Distributions of the parent pair sample (limited to $z > 1.5$) in Gaia BP − RP color (left) and separation (right). The color distributions of DR16Q quasars in the pair ("QSO-DR16Q") and companions classified as "QSO-like" based on proper-motion detection are markedly different from those of companions classified as starlike. The pair separation distributions in the right panel are also different for pairs with QSO-like and starlike companions. In particular, the pair separation distribution for starlike companions drops rapidly toward smaller separation, as expected from the reduction of the geometric cross section of foreground superpositions. In contrast, the pair separation distribution for QSO-like companions is more or less flat across these separations. These distributions are based on the raw pair statistics, without corrections for pair incompleteness toward the subarcsecond regime (see Section 2.3) or removal of the 10 star–quasar superpositions in $<1\farcs5$ pairs based on the PCA (Section 2).

quasar-like companions, especially at $\lesssim 1''$ separations, where the measurement of Gaia proper motion is either unavailable or could be impacted by the close neighbor. We estimate this residual contamination rate using 43 pairs at $<1\farcs5$ separations from the initial sample of 71 double quasars. These pairs are close enough such that the SDSS fiber spectroscopy (with a fiber diameter of $2''$ or $3''$) encloses most light from both components. We use a spectral principal component analysis (PCA) technique to decompose the SDSS spectrum into potential quasar+star superpositions using quasar and stellar PCA templates from the SDSS website. Figure 3 shows that such superpositions can be reliably identified from the SDSS spectrum, provided that the companion is not substantially fainter (e.g., by a factor of ∼10 in flux) than the primary quasar (96.6% of Gaia-resolved pairs in our sample have a flux contrast ratio of <10). However, automatic classifications with PCA-decomposed spectra are often unreliable due to degeneracies in the decomposition and noise in the data. Therefore, we manually inspect all PCA decomposition results and flag obvious star superpositions.

This spectral analysis indicates that there is ∼23% (10/43 in the subset of $<1\farcs5$ pairs) contamination of star+quasar superposition in this subset of pairs. These apparent star superpositions have separations between $0\farcs2$ and $1\farcs2$, with no obvious dependence of the contamination rate on pair separation given the small number statistics. The PCA results for these 10 apparent quasar+star superpositions are shown in Figure 3. We remove these apparent quasar+star pairs from our double quasar sample. There is no way to remove additional stellar contamination in the $>1\farcs5$ pairs without additional follow-up observations. However, the proper-motion measurements are much more reliable for pairs separated by $>1''$ to remove star superpositions in our initial cut. Thus, we expect that the residual contamination rate is substantially smaller than ∼20% at $>1\farcs5$ separations.

The same spectral analysis reveals no obvious, physically unrelated, projected quasar pairs in the $<1\farcs5$ separation subset, in which case, we would observe different emission line redshifts in the spectrum if the redshift difference is $>2000\,\mathrm{km\,s^{-1}}$ (the common definition of projected quasar pairs; e.g., Hennawi et al. 2006, 2010). This is consistent with our expectation from the reduced cross section of chance superpositions for our $<3''$ separation pairs; Hennawi et al. (2010) estimated that ∼30% of the double quasars at $<60''$ separations are projected pairs, which would imply negligible projected pairs at $<3''$ separations. Rare projected quasar pairs are still possible among our wide-separation ($>1\farcs5$) pairs.

After removing foreground star superpositions, most of the remaining 61 pairs should be either genuine dual quasars or gravitationally lensed quasar images. Extended host galaxy emission from old stellar populations at $z > 1.5$ would be too faint to be detectable in the Gaia band, and compact UV-emitting star formation regions in the host galaxy are unlikely to be brighter than our flux limit (which implies quasar luminosities). However, the population of lensed quasars cannot be readily removed. Indeed, resolved Gaia pairs have been used to identify candidate gravitationally lensed quasars and confirmed in follow-up observations (e.g., Lemon et al. 2017; 2018, 2019, 2022b; Krone-Martins et al. 2018). We cross-match the 61 pairs in our sample with the Gravitationally Lensed Quasar Database[12] (Lemon et al. 2019) and the follow-up sample of Gaia DR2-selected candidate lenses and quasar pairs in Lemon et al. (2022b), as well as additional SDSS quasar lens and pair searches (Hennawi et al. 2006; Myers et al. 2008; Oguri et al. 2008; Hennawi et al. 2010; Inada et al. 2012; Kayo & Oguri 2012; More et al. 2016; Eftekharzadeh et al. 2017). We find that there are 25 systems that are reported lenses (but only four of them have image separations of $<1''$) in follow-up observations. There are five systems reported as a physical quasar pair. These publicly reported cases are indicated in the "KNOWN" column in Table 1. It is possible that there are additional sources observed in the literature that are missing from the above resources. Misclassifications of lenses and pairs among these reported cases are rare but possible (see discussions in Section 4.1). Finally, three additional pairs among the 61 (J082341.08+241805.6,

[12] https://research.ast.cam.ac.uk/lensedquasars/; latest version in 2019.

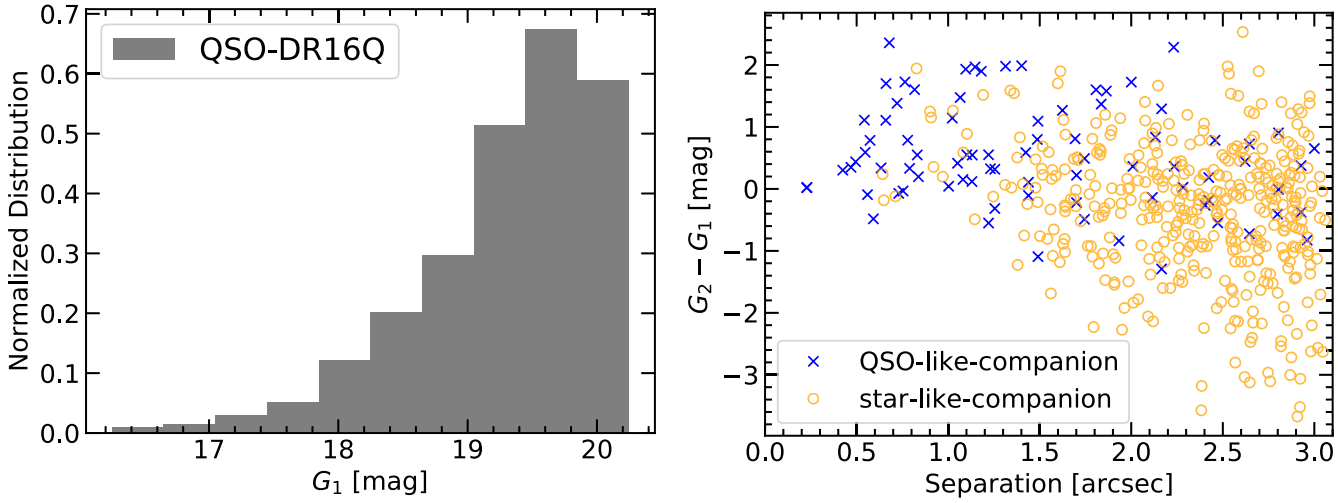


**Figure 2.** Statistical properties of the parent pair sample. Left: $G$-band magnitude distribution for the quasar component in DR16Q ($G_1$) in each pair. Right: magnitude contrast ($G_2$–$G_1$) between the companion and the DR16Q quasar as a function of pair separation. At large separations, the companion can be much brighter than the DR16Q quasar, especially in the case of starlike companions. However, the vast majority of pairs have a flux contrast of less than a factor of 10. As in Figure 1, the pairs here have not been corrected for incompleteness in the subarcsecond regime or cleaned based on the PCA.

J084129.77+482548.4, and J212243.01−002653.8) have been observed in our pilot follow-up with the Hubble Space Telescope (HST; optical and IR) and/or Very Large Array. Objects J0823 and J0841 are confirmed double quasars, more likely dual than lensed quasars (Y. Chen et al. 2022, in preparation). Object J2122 was reported as a dual/lensed quasar based on resolved two-band optical HST color (Chen et al. 2022d), pending further confirmation from additional follow-ups.

While cross-matching our full SDSS+Gaia pair sample (487 pairs) with the above literature on quasar pairs and lenses (as well as our ongoing follow-up), we found that one system (J135306.34+113804.7; 1.″39 separation) classified by us as a quasar–star pair based on Gaia proper motion turns out to be a lensed quasar (Inada et al. 2012). The significance of the proper-motion detection for its companion is PM_SIG2 $\approx 6$, compared to the median significance of 30 for pairs classified as quasar–star pairs based on proper motion. This could be one of the rare cases where the Gaia proper-motion measurement is compromised by a bright close neighbor. On the other hand, only one system (J003337.58+201538.1) classified by us as a double quasar (separated by 1.″69) turns out to be a quasar–star pair based on spatially resolved optical spectroscopy (More et al. 2016). We remove J0033+2015 from further analysis, leaving a final cleaned double quasar sample of 60 objects.

Unfortunately, the completeness of follow-up observations of candidate quasar pairs or lensed quasars is difficult to quantify and varies across different surveys. Moreover, the constraints on the lensed quasar population in the subarcsecond regime are essentially absent. For these reasons, we statistically evaluate the contribution of lensed quasars in our pair sample using mock catalogs, as described in Section 3. Nevertheless, the fact that ∼half of our double quasar sample are already confirmed lensed quasars or quasar pairs indicates that our SDSS+Gaia selection is highly effective, and the resulting sample of 60 objects has a high purity of genuine double quasars.

Figure 4 displays the distribution of these 60 pairs in the redshift-separation space. These double quasars have pair separations between 0.″4 and ∼3″ and form the basis of our subsequent analyses. At the sample median redshift of $z = 2$, these pairs probe projected separations of 3 kpc $\lesssim r_p \lesssim$ 30 kpc, i.e., on galactic scales. Individual pairs may still have 3D separations exceeding 30 kpc, but statistically, this population still traces the radial distribution of quasar pairs. Projection effects are properly taken into account when comparing with theoretical predictions in Sections 3 and 4.

### 2.2. Target Selection Biases

The fact that close photometric companions within 3″ of SDSS quasars are dominated by the foreground (star) population signifies the necessity of additional metrics to remove foreground contamination in quasar pair searches. This high foreground contamination rate is verified in a random offset test. We shuffle the positions of SDSS quasars by 1′ and search for Gaia sources within a 3″ radius circle. This random offset test maintains the foreground stellar density distribution applicable to the SDSS quasar sample. We find a chance star superposition around 0.68% of the quasars when limiting to the same $G < 20.25$ limit of Gaia sources. This is even higher than the ∼0.36% rate for the observed sample above (i.e., 487 Gaia pairs among 134,796 quasars). The main reason for the lower superposition contamination rate in the observed quasar sample is due to SDSS selection. The SDSS quasars were targeted by color selection with photometry (with ∼1.″4 seeing) and spectroscopically confirmed with 2″ or 3″ diameter fiber spectroscopy. The presence of a star brighter than the quasar itself will impact both the target selection and the spectroscopic classification. In this sense, the SDSS quasar sample is biased against close pairs with bright star companions. If we further require $G$ to be no more than 2.5 mag brighter than the quasar in the offset test, we find that 0.47% of the quasars have chance foreground superpositions, roughly consistent with the observed rate. Additional effects, e.g., incompleteness in resolving pairs at <1″, would further reduce the observed foreground contamination rate.

Another complication is that SDSS quasar target selection using SDSS photometry may be biased against double quasars. For $z > 1.5$ double quasars with separations $\gtrsim$1.″4 (typical seeing at the SDSS site), SDSS photometry deblends the pair (two point sources) well, and there is no bias against targeting

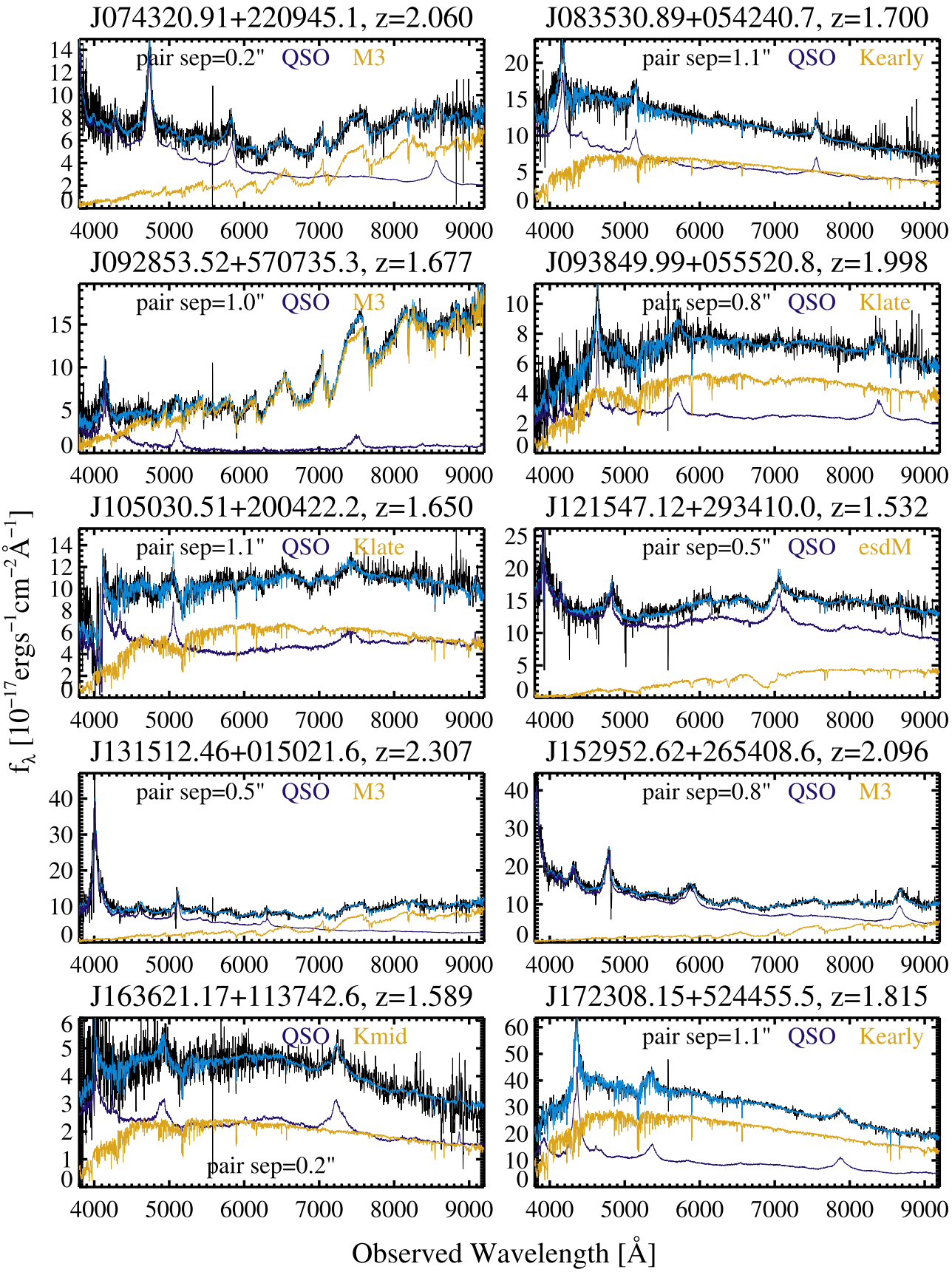


**Figure 3.** Spectral PCA results for the 10 pairs with separations $<1\farcs5$ originally included in our double quasar sample but best explained by star+quasar superpositions based on the SDSS spectra (Section 2). In each panel, the black and cyan lines are the raw and reconstructed spectra, respectively. The blue and orange lines are the decomposed components from the quasar and stellar templates, respectively, with the stellar type indicated in the upper right corner.

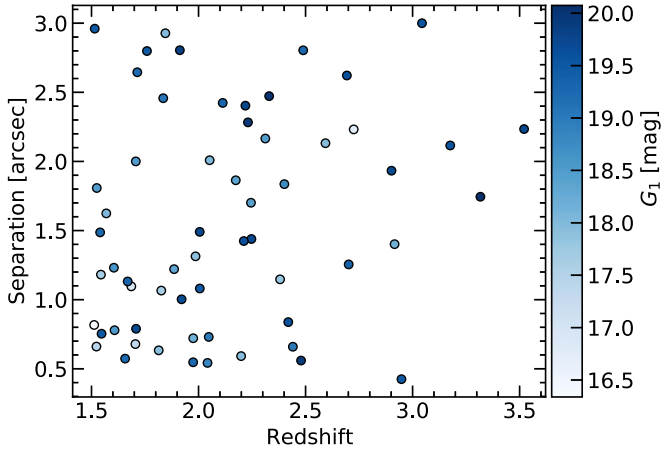


**Figure 4.** Distribution of our final sample of 60 double quasars in the redshift-separation space, color-coded by the $G_1$ magnitude (as listed in Table 1) of each pair.

one or both components of the pair as quasars. If the pair separation is $\lesssim$0.″8, the SDSS photometric pipeline fits a single PSF model to the pair, and the targeting bias against double quasars is also negligible. For pair separations within ∼0.″8–1.″4, the SDSS photometric pipeline cannot readily deblend the pair into two sources, but the profile is also not a point source. Thus, any quasar target selection restricted to point-source objects could potentially miss genuine double quasars in this regime. However, due to a fortuitous combination of factors, this targeting bias does not impact our results much. Our selection requires both components of the pair to have $G < 20.25$ ($i < 20.13$). For this ∼0.″8–1.″4 pair separation range, the SDSS magnitude is $i < 19.35$ (summed flux of the nondeblended pair). In the SDSS legacy survey (SDSS-I/II), quasars were targeted to $i < 19.1$ at $z \lesssim 3$, without the point-source requirement (Richards et al. 2002). Therefore, most of these bright close pairs were already targeted by SDSS-I/II and spectroscopically confirmed. The SDSS-III and SDSS-IV do impose the point-source requirement (Ross et al. 2012; Myers et al. 2015); however, there are also various ancillary quasar target selections that would recover some "single extended sources" in SDSS-III/IV. We have examined the SDSS photometric morphology for quasars in our pair sample, and indeed, some of them are classified as extended sources. From this analysis, we conclude that any targeting bias against double quasars inherent to SDSS selection is insignificant for our pair sample selection. However, for other studies using SDSS quasars targeted to fainter flux limits (i.e., with SDSS-III and SDSS-IV), one should take into account this targeting bias against close (e.g., ∼0.″8–1.″4) double quasars.

### 2.3. Pair Completeness

The raw observed pair statistics as a function of separation (Figure 1, right) suffer significantly from incompleteness in the subarcsecond regime, as Gaia can only resolve the pair at ∼0.″2 resolution in the along-scan direction (this is somewhat remedied by multiple scans along different directions). Moreover, the presence of a close neighbor decreases the probability of detecting both sources photometrically by Gaia. The pair-resolving completeness as a function of separation has been estimated (Fabricius et al. 2021) using the Washington Double Star (WDS) catalog (Mason et al. 2001), demonstrating significant improvements of EDR3 over DR2. Based on the WDS catalog, the pair completeness is ∼50% (20%) at 0.″5 (0.″3) separations. However, the WDS catalog has a different magnitude distribution (i.e., much brighter) than the parent SDSS quasar sample, and it is reasonable to expect that the completeness of Gaia-resolved pairs depends on both magnitude and magnitude contrast. Therefore, we carry out an independent measurement of the pair completeness in Gaia EDR3, as detailed below.

We consider the detectability of close pairs as functions of the magnitude of the brighter primary source, the magnitude difference between the two sources, and their angular separation. There have been previous studies focusing on the Gaia pair completeness as functions of angular separation (Fabricius et al. 2021) and magnitude differences (El-Badry & Rix 2018), but the exact pair completeness depends on the detailed selection criteria of the sample of interest (El-Badry & Rix 2018).

We assemble a random pair sample where the pairs are dominated by random stellar pairs and derive the completeness $f_{\rm comp}$ by comparing the observed number of pairs with the expected number of random pairs from a constant sky density of stars, $Nds \propto sds$, where $s$ is the projected angular separation. Following Hwang et al. (2022b), we collect all pairs in the crowded field at $30° < l < 55°$ and $5° < b < 7°$. This region is chosen such that the Gaia source density is high at low Galactic latitudes, and the region is not strongly affected by dust extinction. We query all Gaia EDR3 sources within this sky region, without any other criteria. Then we collect all pairs with angular separations of <10″. To reduce the binary star contribution, which is more prominent at $G < 16$ (because brighter stars are closer and thus their binary companions are more likely to be spatially resolved), we further impose a cut on parallaxes of <0.5 mas, resulting in 16.7 million unique pairs.

We derive the pair completeness $f_{\rm comp}$ as a function of three parameters: magnitude of the brighter primary ($G_{\rm pri}$), magnitude difference ($\Delta G = G_{\rm sec} - G_{\rm pri}$, where $G_{\rm sec}$ is the $G$-band magnitude of the secondary), and angular separation. To this end, we bin these random pairs by $G_{\rm pri} = 15$–21 with steps of 1 mag, $\Delta G = 0$–3 with steps of 0.5 mag, and angular separations 0.″1–4″ with steps of 0.″2. Then, at each point of the 3D parameter grid, we compute the completeness $f_{\rm comp} = N_{\rm obs}/N_{\rm model}$, where $N_{\rm obs}$ is the observed number of pairs in the grid, and $N_{\rm model}$ is the expected number of pairs from the model. We require $N_{\rm obs} \geqslant 3$ in each bin for completeness calculation.

The model is computed as follows. First, for every primary magnitude bin, we start with the first magnitude difference bin (i.e., $0 < \Delta G < 0.5$) and compute the expected number of pairs along the separation bin based on the observed number of pairs at 5″–10″ and the expected geometric distribution ($Nds \propto sds$). Next, under the assumption that the sample is dominated by random pairs and therefore the magnitude difference distribution is independent of pair separation, we use the magnitude difference distribution from pairs at 5″–10″ as the ground truth and apply this distribution to smaller separations to obtain the expected pair counts as a function of $\Delta G$ at different separations.

Our completeness estimation uses the expected geometric distribution $Nds \propto sds$, which is applicable when the sample is indeed dominated by random pairs in each 3D bin. While the overall sample is dominated by random star pairs in this crowded region (Hwang et al. 2022b), if we naively bin the sample into the 3D grid without the parallax cut, there are some

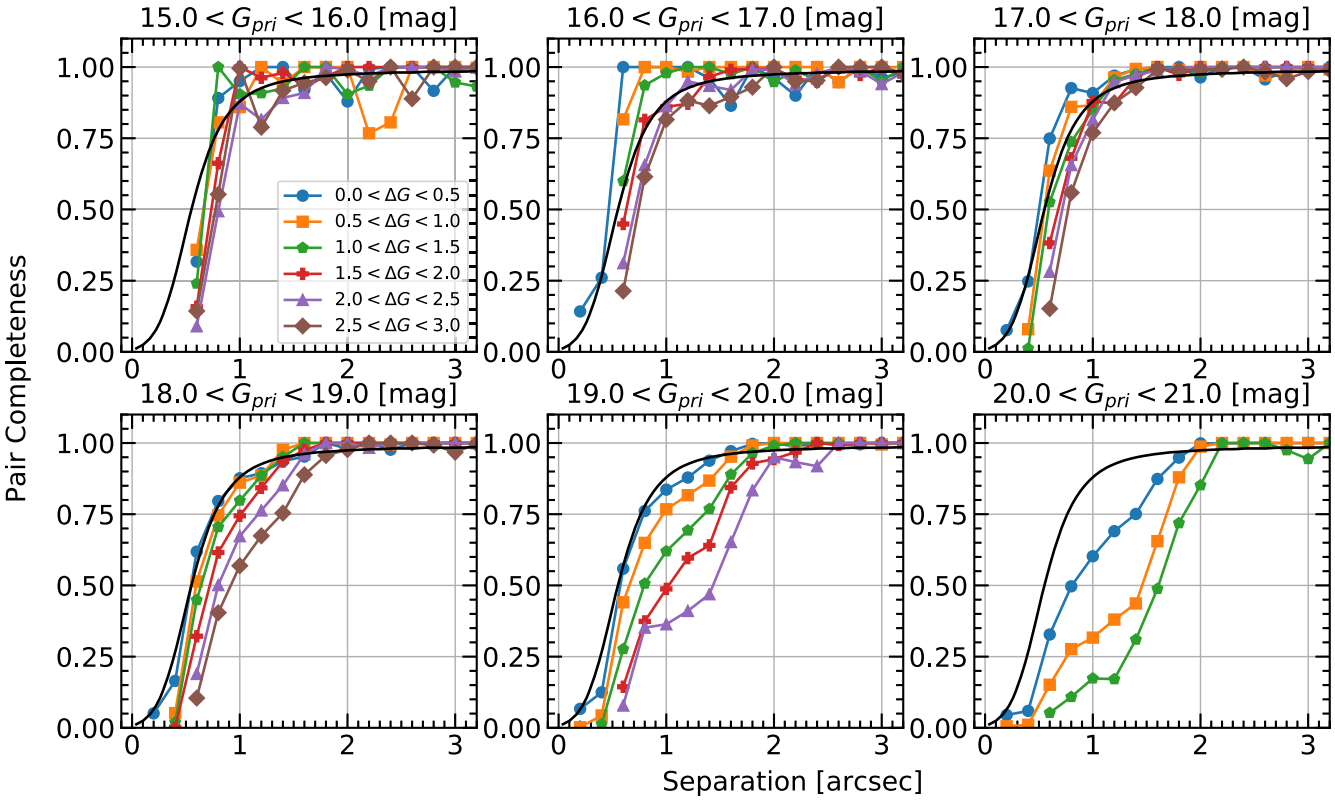


**Figure 5.** Pair completeness as functions of separation, primary magnitude, and magnitude contrast $\Delta G$ estimated using the approach in Section 2.3. The black line is the completeness measured using the WDS catalog from Fabricius et al. (2021).

noticeable binary contributions that cause the completeness >1 at ($G_{\rm pri} < 16$) $\wedge$ ($\Delta G < 0.5$) $\wedge$ (angular separations $<1''$), where $\wedge$ is the logical AND operator. This binary contribution in the observed data is due to the fact that brighter stars are closer, and thus their binary companions are more likely to be resolved by Gaia, producing an excess of "twin" wide binary populations with $\Delta G < 0.25$ (El-Badry et al. 2019; Hwang et al. 2022a). After we remove the nearby stars by the criterion of parallax <0.5 mas, the binary contributions are strongly suppressed, and the completeness is well behaved.

Figure 5 shows the pair completeness as a function of angular separation. Each panel represents a different range of the primary's $G$-band magnitude $G_{\rm pri}$, and each colored symbol is for a different magnitude difference $\Delta G$. For a handful of bins, the completeness estimation can slightly exceed unity due to Poisson fluctuations, and we manually set $f_{\rm comp}$ to 1 in these bins (our quasar pairs rarely fall in these bins anyway). The black lines in Figure 5 are the model-fitted completeness of Gaia EDR3 derived from Fabricius et al. (2021) using the WDS catalog (Mason et al. 2001), which does not take primary magnitudes and magnitude differences into account. The top panels show that our completeness estimation for bright $G_{\rm pri}$ bins agrees well with the black line. At the fainter end of $G_{\rm pri} > 18$, however, our completeness shows that $\Delta G$ plays an important role that is not captured by the black line, emphasizing the importance of deriving the customized completeness correction for our quasar sample. Due to Gaia's detection limit at ~21 mag, only $\Delta G < 1.5$ have completeness available in the $20 < G_{\rm pri} < 21$ panel (bottom right). The pair completeness estimation on the 3D grid of ($G_{\rm pri}$, $\Delta G$, and $\Delta\theta$) is available as an electronic FITS table with its content described in Table 2.

## 3. Results

To calculate the pair fraction, we define the parent quasar sample as the ~134,000 SDSS quasars with the same magnitude and redshift cuts as our pair sample but unresolved by Gaia. The overall abundance of double quasars with separations over ~0.″3–3″ is negligible compared to the parent single quasar population (e.g., even after completeness correction, the total pair fraction over these scales is of order $10^{-4}$–$10^{-3}$). In any case, the parent sample only provides the denominator in the pair fraction calculation and does not affect the relative fraction as a function of pair separation.

We show the completeness-corrected double quasar fraction as a function of angular separation in Figure 6, where the pair fraction is defined as the ratio between the number of pairs in each separation bin and the total number of quasars in the parent sample. In detail, we use the binned completeness estimates $f_{\rm comp}$ over a grid of the $G$ magnitude of the primary, magnitude contrast, and angular separation as quantified in Section 2.3. Each quasar pair in our sample is weighted up by $1/f_{\rm comp}$, and the correction is significant only in the subarcsecond regime. We estimate the uncertainties of the corrected pair statistics using bootstrap resampling of the pairs, which are consistent with the Poisson uncertainties estimated from the raw pair counts in each separation bin (see Table 3). The cumulative pair fraction within 0.″3–3.″1 is $6.2 \pm 0.5 \times 10^{-4}$ among $z > 1.5$ quasars. Dividing these quasar pairs at their median redshift $\langle z \rangle = 2$, we measure overall pair fractions over these scales of $6.6 \pm 1.2 \times 10^{-4}$ and $5.9 \pm 1.0 \times 10^{-4}$ in the lower ($\langle z \rangle = 1.7$) and higher ($\langle z \rangle = 2.4$) redshift bins, respectively, indicating that there is no strong evolution in the pair fraction over the redshift range probed by our sample.

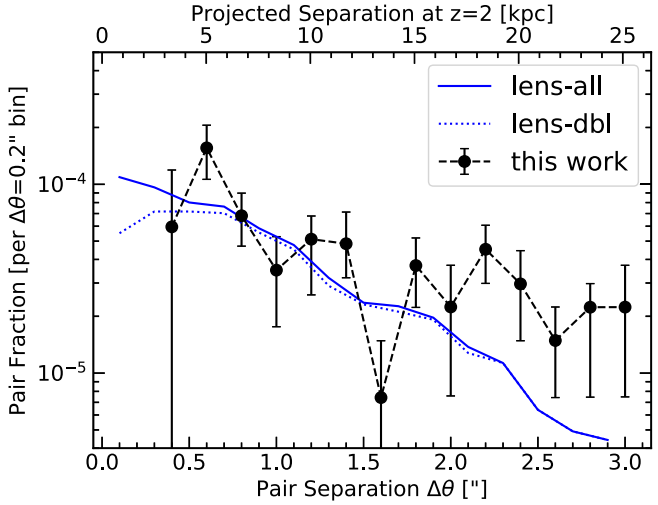


**Figure 6.** Measured quasar pair fraction at $z > 1.5$ and $G < 20.25$ (black circles with error bars), corrected for pair incompleteness (Section 2.3). Pair fraction uncertainties are estimated using bootstrap resampling. For comparison, we show the theoretically predicted lensed quasar fraction (matched in redshift and flux limit to our observed sample) from an updated version of the mock catalog described in Oguri & Marshall (2010) for all lenses (solid blue line) and doubly lensed quasars (dotted blue line), respectively.

**Table 2**
Binned Pair Completeness

| Column (1) | Format (2) | Units (3) | Description (4) |
|---|---|---|---|
| GPRI | FLOAT[2] | mag | Boundary of $G_{\rm pri}$ |
| DG | FLOAT[7] | mag | Boundaries of the $\Delta G$ grid |
| DTHETA | FLOAT[20] | arcsec | Boundaries of the $\Delta\theta$ grid |
| FCOMP | FLOAT[19,6] | | Pair completeness |

**Note.** For each row of the FITS table, GPRI is the boundary of $G_{\rm pri}$, and DG and DTHETA are the boundaries (not bin center) of the $\Delta G$ and $\Delta\theta$ grids in that $G_{\rm pri}$ bin, respectively. The bin size for the $\Delta G$ grid is 0.5 mag, and the bin size for the $\Delta\theta$ grid is $0\farcs2$. The binned completeness FCOMP is set to "NAN" if the observed number of star pairs is <3 in that bin.

(This table is available in its entirety in machine-readable form.)

For completeness, we also present in Table 3 the corrected pair statistics using the pair-resolving completeness estimated in Fabricius et al. (2021) based on the WDS catalog. As demonstrated in Section 2.3, our quasars are substantially fainter than sources in the WDS catalog, and the pair completeness in the subarcsecond regime is somewhat lower than that in Fabricius et al. (2021). Nevertheless, the corrected pair statistics using the completeness in Fabricius et al. (2021) are consistent with our fiducial estimates within $1\sigma$. The uncertainty in the pair statistics is the largest in the smallest $\Delta\theta$ bin, where there is only one observed quasar pair at $0\farcs4$ separation, J0841+4825. This particular pair was first reported in Shen et al. (2021) as a genuine double quasar, although their data were insufficient to rule out the lensed quasar scenario.

As shown in Figure 6, the completeness-corrected double quasar fraction (per linear separation bin) gradually rises toward smaller separations (for reference, $1''$ corresponds to $\sim$8.5 kpc at $z \sim 2$). A constant pair fraction with separation is consistent with a quasar autocorrelation function of $\xi(r) \propto (r/r_0)^{-2}$, where $r$ is the 3D pair distance, and $r_0$ is the correlation length. The steepening of the pair fraction

**Table 3**
Binned Double Quasar Statistics

| $\Delta\theta$ (arcsec) (1) | $N_{\rm QQ}$ (2) | $N_{\rm QQ,\ corr}$ (3) | $\sigma_-$ (4) | $\sigma_+$ (5) | $\sigma_{\rm Poisson}$ (6) | $N_{\rm QQ,\ EDR3}$ (7) |
|---|---|---|---|---|---|---|
| 0.4 | 1 | 8.0 | 8.0 | 8.0 | 8.0 | 3.7 |
| 0.6 | 9 | 21.0 | 6.7 | 6.7 | 7.0 | 15.8 |
| 0.8 | 7 | 9.2 | 2.8 | 2.9 | 3.5 | 9.0 |
| 1.0 | 4 | 4.7 | 2.4 | 2.4 | 2.4 | 4.6 |
| 1.2 | 6 | 6.9 | 3.4 | 2.3 | 2.8 | 6.5 |
| 1.4 | 6 | 6.5 | 2.2 | 3.1 | 2.7 | 6.3 |
| 1.6 | 1 | 1.0 | 1.0 | 1.0 | 1.0 | 1.0 |
| 1.8 | 5 | 5.0 | 2.0 | 2.0 | 2.2 | 5.2 |
| 2.0 | 3 | 3.0 | 2.0 | 2.0 | 1.7 | 3.1 |
| 2.2 | 6 | 6.1 | 2.1 | 2.1 | 2.5 | 6.1 |
| 2.4 | 4 | 4.0 | 2.0 | 2.0 | 2.0 | 4.1 |
| 2.6 | 2 | 2.0 | 1.0 | 1.0 | 1.4 | 2.0 |
| 2.8 | 3 | 3.0 | 2.0 | 1.0 | 1.7 | 3.1 |
| 3.0 | 3 | 3.0 | 2.0 | 2.0 | 1.7 | 3.1 |
| 0.3–3.1 | 60 | 83.5 | 7.1 | 7.5 | ⋯ | 73.5 |

**Note.** Pair statistics are measured in $\Delta\theta$ bins with a linear bin size of $0\farcs2$. Columns (3)–(5) are the pair statistics corrected for completeness ($N_{\rm QQ,\ corr}$), with the uncertainties ($\sigma_-$ and $\sigma_+$) estimated from bootstrap resampling. Column (6) lists the uncertainties in $N_{\rm QQ,\ corr}$ estimated from Poisson counting uncertainties from the raw pair counts $N_{\rm QQ}$. Column (7) lists the corrected pair counts using the estimated completeness in Fabricius et al. (2021), which remains less than unity even at $\Delta\theta > 2''$.

toward small separations implies a steepening in small-scale quasar clustering at $\lesssim$30 kpc physical scales.

Not all pairs in our final cleaned sample of 60 systems are physical quasar pairs, as some of them should be gravitationally lensed quasars. The lensed quasar statistics in the subarcsecond regime is not well constrained observationally; therefore, we use an updated mock catalog of lensed quasars from Oguri & Marshall (2010) to estimate the lensed quasar contribution (see also Lemon et al. 2022b). The updated version uses a galaxy velocity dispersion function for all types of galaxies (in contrast to only early-type galaxies considered in the original version of the mock) and imposes no lower limit on the image separation (in contrast to the lower limit of image separation of $0\farcs5$ in the original version of the mock).

We include all lensed systems (e.g., doubles, quads, etc.) in the mock catalog with two (and only two) images above the flux limit, with the same redshift cut of $z > 1.5$ as for our observed sample. The mock catalog uses SDSS $i$-band magnitude, and we adopt $i < 20.2$ for individual resolved images that roughly correspond to the same $G$-band limit used for the observed pair sample. Varying the flux limit in the mock lensed quasar catalog by 1 mag introduces less than a factor of 2 in the lensed quasar fractions. Lensed quasars with more than two images above the flux limit would not have been included in our pair sample. The lensed quasar fraction (blue lines in Figure 6) also shows a gradual increase toward the subarcsecond regime, mainly due to the increase in the abundance of less massive lens galaxies.

In Figure 7, we compare our double quasar fraction with predictions for dual AGNs at $z \sim 2$ in the cosmological hydrodynamic simulation ASTRID (Chen et al. 2022b). ASTRID is a recently developed large-volume, high-resolution (with a gravitational softening of 1.5 kpc $h^{-1}$ and a dark matter mass resolution of $9.6 \times 10^6\,M_\odot$) cosmological hydrodynamic simulation that studies the evolution of galaxies and SMBHs. It utilizes a new version of the MP-Gadget (Feng et al. 2018)

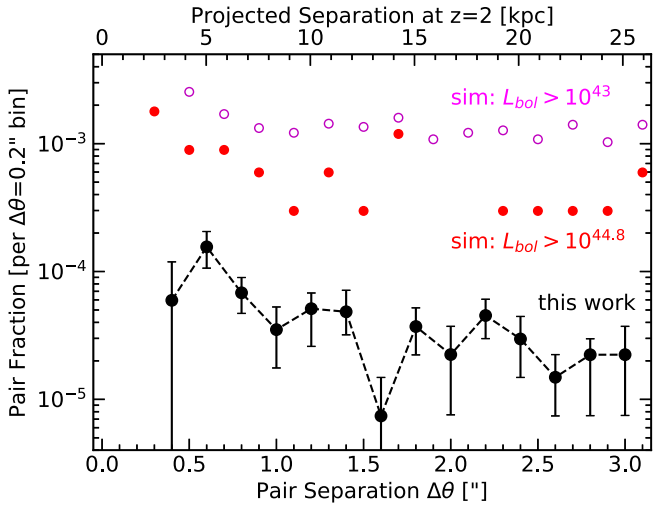


**Figure 7.** Same as Figure 6 but for the comparison between observed AGN pair statistics (black circles with error bars) and predictions from the ASTRID cosmological simulation (magenta and red points) at $z \sim 2$ (Chen et al. 2022b). The simulated sample only has statistics to probe AGNs that are at least 10 times fainter than our quasar sample and includes both unobscured and obscured AGNs.

simulation code to solve the gravitational evolution (with an $N$-body tree-particle-mesh approach), hydrodynamics (with smoothed particle hydrodynamics), and astrophysical processes with a series of subgrid models. With a comoving volume of $(250\,\mathrm{Mpc}\ h^{-1})^3$, ASTRID is the largest galaxy formation simulation to date that covers the epoch of the cosmic noon. The large volume of ASTRID can provide a statistical sample of the rare quasar population, and the high resolution enables detailed studies of the quasar pair statistics and environments down to galactic scales. Details of the ASTRID simulation and the SMBH population overview can be found in Bird et al. (2022), Ni et al. (2022), and Chen et al. (2022c), and a comprehensive analysis of the dual AGN population predicted by ASTRID can be found in Chen et al. (2022c, 2022b).

Given the simulation volume of ASTRID, we can only explore dual AGNs with lower luminosities than our quasar sample. For instance, there are three dual AGNs at $z \sim 2$ in ASTRID that sample the same luminosity and pair separation ranges as our observed sample, which is not enough for detailed statistical analysis. We therefore use two lower bolometric luminosity cuts, $L_{\rm bol} > 10^{44.8}$ and $10^{43}\,\mathrm{erg\,s^{-1}}$, to select the parent single and dual AGNs in ASTRID. We impose a black hole (BH) mass cut of $M_{\rm BH} > 10^7\,M_\odot$ in the simulated AGNs; this BH mass scale is resolved in ASTRID. The simulated dual AGNs are restricted to having radial separations of $<50$ kpc and transverse separations of $<30$ kpc. The resulting simulated dual AGN sample includes 59 and 1282 pairs for the two luminosity cuts, respectively. As shown in Figure 7, the dual AGN fraction is generally lower for the higher-luminosity cut. Nevertheless, both simulated samples show an enhancement in the pair fraction toward the smallest separations, as seen in the observed sample.

If we could increase the luminosity threshold further in the simulated AGN sample, as pair statistics allow, we would expect to see a further reduced dual fraction. This luminosity trend in the dual AGN fraction can be qualitatively understood as follows. If assuming no merger-enhanced AGN duty cycles $f(L_{\rm min})$, the dual AGN fraction (among all AGNs with the same luminosity threshold $L_{\rm min}$) depends on $L_{\rm min}$ through the duty cycle, i.e., $\propto f(L_{\rm min})$, while the fraction of pairs with a single AGN among all AGNs is constant with the luminosity threshold. As $L_{\rm min}$ increases, the duty cycle $f(L_{\rm min})$ decreases, leading to a reduced dual AGN fraction among all AGNs. The average AGN duty cycle at $z \sim 2$ in the ASTRID simulation (for all $M_{\rm BH} > 10^7\,M_\odot$ SMBHs) roughly decreases by a factor of 10 from $L_{\rm bol} > 10^{43}$ to $10^{44.8}\,\mathrm{erg\,s^{-1}}$ and by another factor of $\sim$10 from $L_{\rm bol} > 10^{44.8}$ to $10^{45.8}\,\mathrm{erg\,s^{-1}}$ (N. Chen et al. 2022, in preparation). Thus, we expect that the simulated dual AGN fraction for $L_{\rm bol} > 10^{45.8}\,\mathrm{erg\,s^{-1}}$ (matching our observed sample) would be a factor of $\sim$10 smaller than the red points in Figure 7, which would match the observed statistics. However, we do expect somewhat enhanced AGN duty cycles in galaxy mergers, which would elevate the simulated dual AGN fraction.

The above comparison with simulations should be interpreted with some caution. First of all, currently, the simulated sample does not distinguish between obscured and unobscured AGNs, while our quasar sample only contains unobscured objects. Simulations at $z \sim 2$ have shown that many luminous dual AGNs are completely obscured in gas-rich mergers (Chen et al. 2022b), which would significantly reduce the observable fraction of unobscured dual quasars. Second, it might be necessary to further match the SMBH masses in this comparison; i.e., the observed SDSS quasars have BH masses $>$a few $\times\ 10^8\,M_\odot$ (e.g., Shen et al. 2011). In any case, we conclude that the observed double quasar statistics are roughly consistent with predictions for the dual AGN population from simulations.

The intriguing finding that the observed double quasar statistics are consistent with theoretical predictions for both lensing and simulated dual AGNs may indicate that these two populations are comparable in number by coincidence. A complete division between lenses and dual quasars in our sample with follow-up observations will fully address this important issue. We further discuss the implications of our observed pair statistics in Section 4.

Our definition of the quasar pair fraction is free of a selection bias related to the flux limit and source blending. When selecting a sample of unresolved systems (either single quasars or unresolved pairs), potential pairs or lensed images would boost the combined flux to above the flux limit and enhance the presence of pairs in the parent sample. In the case of gravitational lenses, this is the magnification bias. However, our Gaia sample is a resolved pair sample, and each component of the pair is above the flux limit. In other words, our pair fraction is defined as the fraction of $G < 20.25$ quasars that have a resolved quasar companion that is also brighter than $G = 20.25$. Pairs with either of the components fainter than the flux limit, even if the other component or the combined flux is above the flux limit, would not have been included in our pair sample to contribute to the numerator. The parent quasar sample has the same flux limit and could include fainter pairs or lensed images that boost the combined fluxes above the threshold, but such small-scale pairs/lensed images are rare and would only slightly perturb the denominator in our pair fraction calculation.

We next examine the flux ratios of the observed quasar pairs. The sample statistics is insufficient to explore the flux ratios as a function of separation in detail; hence, we focus the discussion on the distribution for the full quasar pair sample with $\Delta\theta < 3''$. However, when dividing the quasar pair sample

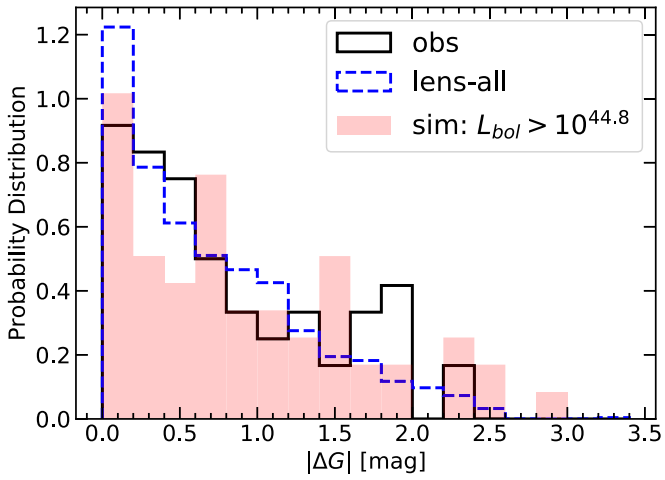


**Figure 8.** Pair flux ratio (or magnitude contrast) distribution of the 60 double quasars in our sample (black solid histogram). The predictions for lensed quasars using the mock catalog in Oguri & Marshall (2010) and for dual AGNs in the cosmological hydrodynamic simulation ASTRID (Chen et al. 2022b) are shown with the blue dashed and pink shaded histograms, respectively.

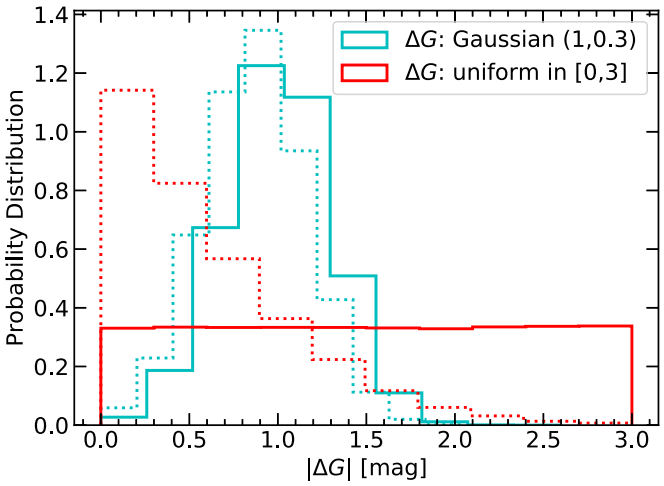


**Figure 9.** Effects of the flux limit ($G < 20.25$) on the observed pair flux ratio distribution. The magnitude distribution of the primary quasar follows the observed distribution. The cyan and red solid histograms show two intrinsic flux ratio distributions: (1) a Gaussian distribution of $\Delta G$ with a mean and dispersion of 1 and 0.3 mag and (2) a uniform distribution of $\Delta G$ over [0,3] mag. The dotted histograms show the resulting observed flux ratio (magnitude contrast) distribution in each case. The flux limit imposed on both components of the pair enhances the prominence of the peak toward an equal flux ratio. If the intrinsic flux ratio distribution is broad (i.e., in the uniform distribution case), selection effects due to the common flux limit would produce a strong peak near an equal flux ratio.

into wide-separation ($\Delta\theta > 1''$) and close-separation ($\Delta\theta < 1''$) pairs, there is no noticeable difference in the pair flux ratio distribution. Figure 8 shows that the observed quasar pair flux ratio distribution peaks near unity.

The flux limit ($G < 20.25$) in our sample selection reduces the dynamic range in the flux ratio of the observed pairs, biasing the distribution of flux ratios toward more equal flux values. To illustrate this effect, we consider the wide-separation ($1'' < \Delta\theta \lesssim 3''$) quasar pairs in our sample, since this subset does not suffer from pair-resolving completeness as much as the close-separation pairs do (Section 2.3). In other words, the main selection effect is due to the flux limit $G < 20.25$ for both components of the pair. In Figure 9, we demonstrate the effect of the flux limit with simple, idealized simulations with an assumed intrinsic flux ratio ($\Delta G$) distribution (solid lines). The magnitude distribution of the primary (brighter) component follows the observed distribution (Figure 2). We test two different input $\Delta G$ distributions: (1) a Gaussian distribution with mean $\Delta G = 1$ (mag) and a dispersion of 0.3 mag and (2) a uniform distribution of $\Delta G$ within [0,3] mag. When the input $\Delta G$ distribution narrowly peaks at a nonequal ratio value (the Gaussian distribution case), the observed pair flux ratio distribution (dotted lines) is slightly shifted to smaller values, but the peak is more or less preserved. On the other hand, if the input distribution is broad (the uniform distribution case), the resulting observed $\Delta G$ distribution peaks at the equal flux ratio.

In Figure 8, we show the AGN pair flux ratio distribution from the ASTRID simulation at $z \sim 2$ (Chen et al. 2022c), again restricting to physical AGN pairs with transverse separations $r_p < 30$ kpc and radial separations $<50$ kpc. Because the AGN population in the simulations is limited by the simulation volume, we relax the luminosity threshold for both components to be $L_{\rm bol} > 10^{44.8}$ erg s$^{-1}$. The pair flux ratios from the simulated AGN pairs also peak around the equal flux ratio, although the peak is somewhat less prominent than that of the observed sample. If we lower the luminosity threshold in the simulated sample, more pairs with large luminosity ratios will be included in the sample, further weakening the peak prominence at the equal flux ratio. Similarly, if we increase the luminosity threshold to match our sample ($L_{\rm bol} > 10^{45.8}$ erg s$^{-1}$), we expect that simulated dual AGNs would produce a prominent peak around the unity flux ratio, similar to the observed distribution. The intrinsic pair flux ratio distribution (for the SMBH pair population) from the simulations, however, is much broader if we relax the flux limit on the fainter component. Synchronized growth of the pair of SMBHs that rapidly drives their masses toward equality does not seem to be the case on these $<$tens of kiloparsec scales.

Finally, we show the flux ratio of lensed quasar images in Figure 8, using the same mock catalog described above. Coincidently, flux ratios of lensed quasar images also peak around the unity flux ratio. This peak is primarily due to selection effects. Double lenses with large magnification factors (which tend to have small magnitude contrasts) from intrinsically fainter quasars are overrepresented in the flux-limited sample due to the lensing magnification bias. Quad lenses often have two bright images with similar magnifications near the critical curve, and this population preferentially resides in the small-separation regime. The magnification bias would also enhance the presence of equal-flux quad lenses (only the two brightest images) in the flux-limited sample. Therefore, the observed pair flux ratio distribution cannot be used to readily distinguish the lensing and quasar pair scenarios in the statistical sense.

## 4. Discussion

Since we focus on luminous quasars at $z > 1.5$ with bolometric luminosities $L_{\rm bol} > 10^{45.8}$ erg s$^{-1}$, and the bulk of the sample is near the flux limit, we make the assumption that the intrinsic quasar pair fraction (as a function of separation) is more or less constant over the luminosity range probed in this work. This simplifies most of the following discussions. The luminosity dependence of pair statistics will be explored in

future work with improved sample statistics and a more extended dynamic range in quasar luminosity.

### 4.1. Lensing versus Pairs

Figure 6 shows that the measured quasar pair fraction in our Gaia sample agrees well with the predicted lensed quasar population at $<1\farcs5$ separations. However, we caution that the lensed quasar fraction is based on mock catalogs and may be different from the actual lensed quasar population at these small separations. In reality, the observed quasar pairs are comparable in number to lensed quasars over few arcsecond separations (e.g., Hennawi et al. 2006, 2010; Kayo & Oguri 2012), but the relative numbers between lensed quasars and pairs are unconstrained at $\lesssim 1''$. There is also an observational bias that preferentially removes subarcsecond lensed quasars from the observed pair sample: lensed quasars are associated with lensing galaxies, which could (if the lensing galaxy is at $z \lesssim 1.5$) change the optical colors of the unresolved system and reduce the probability of selection from ground-based surveys such as the SDSS. Therefore, we expect that at least some of these double quasars are genuine pairs rather than lenses. This is indeed the case, as there are already several confirmed quasar pairs in our sample from the literature, as discussed in Section 2.1.

Follow-up observations of the full sample of 60 double quasar systems will conclusively reveal the division between lensed quasars and physical pairs over the full range of $\sim 0\farcs3$–$3''$ separations. It is notoriously difficult to distinguish these two scenarios at high redshift and small separations (e.g., Shen et al. 2021; Yue et al. 2021). Minor spectral dissimilarities between the two components of the pair are insufficient to rule out lensing (e.g., Shen et al. 2021), while spectral similarities are equally insufficient to rule out a quasar pair, since different quasars can look similar in their spectral appearances (e.g., Rochais et al. 2017), particularly at $z > 1.5$, where optical spectroscopy only covers the rest-frame UV broad lines. Spatially resolved near-IR spectroscopy may be able to reveal the differences in the narrow emission lines, e.g., [O III] 5007, in a quasar pair but is challenging given the signal-to-noise ratio requirement and relatively weak narrow-line emission in high-$z$, high-luminosity quasars (e.g., Shen 2016).

Multiwavelength coverage of the two resolved components may help reject the lensing scenario if the spectral energy distributions are markedly different, e.g., with additional high-resolution radio imaging of the resolved pair. The most decisive and efficient observation to rule out lensing, however, is probably the nondetection of a potential lens galaxy in deep imaging. In the case of $z > 1.5$ candidate quasar pairs at subarcsecond separations, this test requires high spatial resolution and deep IR imaging, ideally from HST or JWST. Indeed, existing optical imaging data (even taken with HST) are too shallow to rule out the lensing hypothesis (e.g., Shen et al. 2021; Chen et al. 2022d) for $z > 1.5$ double quasars, even though statistics may slightly favor the dual quasar scenario over lensing (Shen et al. 2021). High-$z$ lens galaxies will be faint in the optical, and the nondetection limit of the lens placed by HST optical imaging is not stringent enough. For larger-separation pairs, deep IR imaging from ground would be sufficient to rule out (or confirm) the lensing scenario based on the nondetection (or detection) of a lens galaxy. Deep IR imaging may also be able to reveal tidal features in the host of the pair, offering additional evidence for physical merging pairs.

In what follows, we remain agnostic about the division between lensing and pairs in our sample and discuss different outcomes if one or the other population dominates our pair sample.

### 4.2. Dynamical Friction, Quasar Duty Cycles, and Recoiling SMBHs

The overall double quasar fraction from our sample, $f_{\rm QQ} \sim 6 \times 10^{-4}$ ($r_p \sim 3$–$30$ kpc) among all $G < 20.25$ quasars at $\langle z \rangle \approx 2$, is lower than the dual AGN fraction ($\sim 10^{-2}$) at similar redshifts and separations predicted from recent hydrodynamic simulations (e.g., Dubois et al. 2014; Hirschmann et al. 2014; Steinborn et al. 2016; De Rosa et al. 2019; Rosas-Guevara et al. 2019; Volonteri et al. 2022, and references therein). The main reason for this apparent discrepancy is that these simulations do not have sufficient volume to probe the most luminous quasars and thus focus on the much less luminous AGN population ($L_{\rm bol} > 10^{43}\,{\rm erg\,s^{-1}}$). These low-luminosity AGNs have much higher duty cycles than luminous quasars. In general, the dual AGN fraction among AGNs increases as the luminosity threshold decreases, as seen in the simulations (Figure 7), as well as the observed high dual AGN fraction ($\gtrsim$a few percent) among low-luminosity AGNs in the nearby universe (Liu et al. 2011; Koss et al. 2012). Improvements in both the observed sample (to fainter flux limits) and the simulation volume over the next few years will enable a better comparison.

A substantial fraction of AGNs in these simulations are also optically obscured and would not be included in our sample. If obscuration occurs more often in merging pairs than in single AGNs, the dual AGN fraction for the unobscured population will be reduced compared with that for all AGNs. Even if the obscured fraction is the same among single AGNs and AGNs in pairs, requiring both AGNs in the pair to be unobscured would also lead to a reduced dual AGN fraction for unobscured AGNs (similar to the duty cycle argument).

On the observational side and focusing on quasar luminosities ($L_{\rm bol} \gtrsim 10^{45}\,{\rm erg\,s^{-1}}$), Kayo & Oguri (2012) reported a dual quasar fraction of $\sim 5 \times 10^{-4}$ over $0.6 < z < 2.2$ and 10 kpc $\lesssim r_p \lesssim 100$ kpc, which is roughly in line with our measured double quasar fraction over smaller separations and higher redshifts. On the other hand, using ground-based optical imaging of resolved pairs around SDSS quasars from the Hyper Suprime-Cam Subaru Strategic Program, Silverman et al. (2020) reported a double quasar fraction (dual and lensed quasars combined) of $0.26\% \pm 0.18\%$ (requiring a pair flux ratio $>0.1$) over $r_p = 3$–$30$ kpc with no redshift evolution, which is a factor of $\sim 4$ higher (albeit still within $\sim 1\sigma$) than our pair fraction over the same separations. There is a slight difference in the selection of double quasars between our work and that of Silverman et al. (2020); while the flux limit of the primary SDSS quasar is the same, we require the companion to also be brighter than this flux limit, while Silverman et al. (2020) includes companions that can be 10 times fainter than the primary SDSS quasar. Therefore, we expect that some of the double quasars (candidates) in Silverman et al. (2020) would not pass our selection. Similarly, the only lensed dual quasar, J1721+8842 at $z = 2.4$, reported in Lemon et al. (2022a) has a companion too faint to be selected by our criteria.

Furthermore, the Silverman et al. (2020) measurement is based on a ground-based imaging pair sample with loose color selection of quasars, and spectroscopic follow-up is required to remove foreground star contamination in these apparent pairs, as acknowledged by Silverman et al. (2020). Our earlier results based on HST imaging and spectroscopic follow-up of high-redshift candidate quasar pairs have shown that such stellar contamination is significant (e.g., >50%) for pure photometric color selection (Chen et al. 2022d). Foreground star contamination would also be a problem in other predominantly imaging samples of dual/offset AGN candidates (Stemo et al. 2021). In our SDSS+Gaia approach, the additional proper-motion information and the rejection of foreground star superpositions with spectral PCA delivered a much cleaner double quasar sample.

The relative frequency of quasar pairs as a function of separation in the $r_p \sim 3$–30 kpc regime is determined by the dynamical friction timescale and the duty cycle of quasar activity in mergers, both of which are functions of separation. If the quasar duty cycle remains constant over these separations, simple prediction from dynamical friction implies a roughly constant pair fraction per linear separation bin toward smaller separations (e.g., Yu 2002; Chen et al. 2020).

If the pair statistics shown in Figure 6 are dominated by physical quasar pairs, then the rising pair fraction (per linear separation bin) toward small separations indicates that the quasar duty cycle is elevated toward smaller separations, or that the dynamical friction timescale deviates from the scaling predicted in analytical calculations by, e.g., Chen et al. (2020). The observed rising quasar pair fraction toward small separations for our high-redshift ($z > 1.5$) sample is consistent with observations at $z < 1$, where the AGN pair fraction also increases toward small separations at $r_p \lesssim 30$ kpc (e.g., Ellison et al. 2011; Liu et al. 2012; Stemo et al. 2021). Such an elevation of SMBH accretion at small pair separations, i.e., late stages of galaxy mergers, is also seen in some hydrodynamic simulations (e.g., Capelo et al. 2017).

On the other hand, if the pair statistics shown in Figure 6 are dominated by lensed quasars, and the intrinsic physical pair fraction is flat or even decreasing toward smaller separations, it would imply little enhanced (or even reduced) quasar activity toward the ∼kiloparsec regime in galaxy mergers, which would be at odds with numerical simulation and low-redshift observational results. Alternatively, it may imply that at $z \sim 2$, pairs of SMBHs decay more rapidly toward the ∼kiloparsec regime than predicted by dynamical friction from stars, for example, accelerated by the presence of gas (e.g., Callegari et al. 2009) expected in high-redshift gas-rich mergers or the buildup of a dense nuclear stellar cusp around one or both SMBHs (e.g., Van Wassenhove et al. 2014).

Either way, our sample of 60 double quasars can be used to address these different scenarios and constrain the dynamical friction evolution of the SMBH pair, as well as the duty cycle of quasar activity in mergers. To that end, we are conducting follow-up observations to differentiate the pairs versus lensing scenarios for our sample and will present the results in future work.

We end this section by pointing out the possibility that a tiny fraction of these quasar pairs might contain an accreting recoiled SMBH from the prior merger of two SMBHs (e.g., Blecha et al. 2016, and references therein). However, there are still significant theoretical uncertainties on this putative population of recoiling SMBHs and observational challenges to distinguish them from inspiraling SMBHs in galaxy mergers. Perhaps host galaxy properties can be useful to identify recoiling SMBHs as offset AGNs, e.g., if these rogue SMBHs predominately reside in early-type galaxies long after the merger.

### 4.3. FDM and a Possible ∼Kiloparsec Pileup

In the FDM model and ignoring baryonic effects, SMBH pairs in galaxy mergers will stall at $\lambda_{\rm FDM} \sim$ kpc scales due to energy injection from fluctuations of dark matter particles on their de Broglie wavelength $\lambda_{\rm FDM}$ (e.g., Hui et al. 2017). If the duty cycle of quasar activity is independent of pair evolution, we expect to see a dramatic pileup of quasar pairs near the stall distance because these pairs spend a much longer time there (i.e., ∼a Hubble time) compared to their lifetime during the previous galactic inspiral. Our quasar pair sample does not yet well probe the <1 kpc regime, and we do not observe any sudden spike in the pair fraction toward $\sim 0\farcs2$ (corresponding to ∼1.6 kpc at $z \sim 2$). Pair statistics with future data sets (see Section 5) will probe the subkiloparsec regime and constrain the nature of FDM.

However, absence of evidence is not evidence of absence. The potential lack of a pileup of quasar pairs below ∼1 kpc can be explained by baryonic effects; i.e., the pair orbit can further decay regardless of the energy pumping from FDM fluctuations. In addition, in the final stage of pair evolution, long after the initial galaxy merger, accretion onto SMBHs may become much less efficient, leading to a diminished fraction of dual quasars among these stalled ∼kiloparsec SMBH pairs. The most exciting aspect of this test is to potentially reveal that there is indeed a pileup of quasar pairs on $\lesssim$kiloparsec scales, which would offer strong support to the FDM model. Compared to other observational tests (Hui et al. 2017), the statistics of ∼kiloparsec-scale quasar pairs offer a simple but potentially definitive test (but see below), hinging on the discovery of such a pileup of SMBH pairs.

On the other hand, certain dynamical processes associated with baryonic matter might also lead to the stalling of SMBH pairs at ∼kiloparsec scales (Amaro-Seoane et al. 2022, and references therein). For example, in the case of massive (e.g., $>10^7\,M_\odot$) SMBHs, clumpiness in the host galaxy and inhomogeneous gas and stellar density profiles can lead to inefficient inspiral and potentially stalling of the SMBH pair at ∼kiloparsec separations (e.g., Tamburello et al. 2017; Pfister et al. 2019; Bortolas et al. 2020). This is still in early theoretical investigations, and observations of host galaxies of high-redshift dual quasars might offer insights on these dynamical processes.

## 5. Conclusions

In this work, we have measured the quasar pair statistics over $\sim 0\farcs3$–$3''$ separations at $z > 1.5$ (median redshift $\langle z \rangle \approx 2$) using a sample of 60 resolved double quasars from Gaia EDR3 (Fabricius et al. 2021). These pairs are selected by cross-matching the Gaia EDR3 catalog with spectroscopically confirmed quasars from SDSS DR16 (Lyke et al. 2020). Both members of the pair are flux limited to $G < 20.25$; therefore, our pair sample corresponds to the luminous quasar population at cosmic noon, with $L_{\rm bol} > 10^{45.8}\,{\rm erg\,s^{-1}}$ at $z > 1.5$. We efficiently separate quasars and stars in resolved pairs using

Gaia proper-motion measurements and PCA of SDSS spectra (Section 2.1). We quantify the pair completeness in Gaia EDR3 as functions of pair separation $\Delta\theta$, magnitude of the primary, and magnitude contrast of the pair (Section 2.3). The completeness-corrected pair fraction (per linear separation bin; among all $z > 1.5$ quasars at $G < 20.25$) increases toward smaller separations and is elevated by a factor of $\sim$5 from $\Delta\theta \sim 3''$ to $0\farcs3$. The integrated pair fraction over $\sim 0\farcs3$–$3''$ scales (corresponding to projected physical separations of $\sim$3–30 kpc at $z \sim 2$) is $\sim 6.2 \pm 0.5 \times 10^{-4}$, with no obvious evolution in the redshift range of our sample.

The major caveat of the current analysis is that the division between physical quasar pairs and gravitationally lensed quasars is unknown, especially in the subarcsecond regime. Previous searches of high-redshift quasar pairs and lensed quasars on $>1''$ scales have revealed that both populations contribute significantly to the observed double quasars (e.g., Hennawi et al. 2006; Myers et al. 2008; Hennawi et al. 2010; Kayo & Oguri 2012; More et al. 2016; Eftekharzadeh et al. 2017). It is then reasonable to expect that there are both bona fide quasar pairs and lensed quasars in the subarcsecond regime. We are conducting follow-up observations for the complete sample of 60 double quasars presented here and will refine our constraints on the quasar pair statistics.

This work represents a meaningful advance on observational constraints on the formation and evolution of SMBH pairs at high redshift. Granted, the depth of Gaia and SDSS limits such a systematic search to the most luminous quasars, missing the bulk of rapidly growing SMBHs at cosmic noon. The important and more abundant populations of single offset AGNs in mergers and obscured AGNs are also not explored with the Gaia+SDSS sample. Nevertheless, this approach with Gaia +SDSS has delivered some of the first statistical measurements of quasar pair fractions in a redshift-separation regime that has just started to be explored in a systematic fashion (e.g., Silverman et al. 2020; Stemo et al. 2021; Chen et al. 2022d). With continued Gaia observations (more resolved pairs from different scanning directions), we expect to recover additional luminous quasar pairs at $z > 1.5$ to improve the statistics.

However, the intrinsic abundance of luminous quasar pairs at cosmic noon is low. In order to significantly improve the pair statistics, extend to lower AGN luminosities, and explore the diversity in SMBH and host properties, it is necessary to carry out similar searches with deeper, wide-area surveys at subarcsecond resolution. Upcoming wide-field space missions, such as Euclid (Scaramella et al. 2022; to be launched in $\sim$2023), the Chinese Space Station Telescope (Zhan 2021; to be launched in $\sim$2024), and the Nancy Grace Roman Space Telescope (Roman, Spergel et al. 2015; to be launched before $\sim$2027), will provide the perfect combination to perform systematic searches of SMBH pairs across cosmic time. All three missions will carry out a wide-field imaging survey in multiple filters with $\sim 0\farcs05$–$0\farcs2$ resolution and depths of $\sim$25–28 AB mag, with additional spectroscopic capabilities. The combined photometric data cover a broad wavelength range across the UV–optical–near-infrared. These data can be used to efficiently select candidate quasar pairs based on photometric colors and spectroscopic information, down to the diffraction limit of these space telescopes. Dedicated follow-up observations of these candidates can confirm the nature of these pairs, if needed.

In particular, the deep IR imaging from Euclid and Roman will be useful to test the lensing scenario for high-redshift double quasars. In addition, the capability of detecting the host galaxy in deep IR imaging and measuring the subarcsecond offset of the point sources within will enable the systematic discovery of single offset AGNs in high-redshift mergers. Host galaxy measurements will also allow a detailed look at the populations of dual and offset AGNs in different types of galaxies, shedding light on AGN fueling and recoiling SMBHs. With combined data sets from these upcoming space-based surveys, we will conclusively measure the abundances of galactic-scale quasar and AGN pairs, offset AGNs, and subarcsecond lensed quasars across most of the cosmic history, with unprecedented statistics and coverage of the parameter space of SMBHs and host galaxies.

We thank the anonymous referee for useful comments that improved the manuscript and P. Capelo, Lucio Mayer, Joe Hennawi, and Cameron Lemon for useful discussions. This work is partially supported by NSF grants AST-2009947 (Y.S.) and AST-2108162 (Y.S., X.L.). M.O. acknowledges support by JSPS KAKENHI grant Nos. JP22H01260, JP20H05856, and JP20H00181. H.C.H. acknowledges the support of the Infosys Membership at the Institute for Advanced Study. N.L. Z. acknowledges support by NASA through grant HST-GO-15900 from the Space Telescope Science Institute and by the Institute for Advanced Study through a J. Robbert Oppenheimer Visiting Professorship and the Bershadsky Fund. This research was supported in part by the National Science Foundation under grant No. PHY-1748958. We are grateful for the hospitality of the Kavli Institute for Theoretical Physics at UC Santa Barbara and the KITP Conference Building Bridges: Toward a Unified Picture of Stellar and Black Hole Binary Accretion and Evolution (2022 May), during which part of the work was performed.

## ORCID iDs

Yue Shen https://orcid.org/0000-0003-1659-7035
Hsiang-Chih Hwang https://orcid.org/0000-0003-4250-4437
Masamune Oguri https://orcid.org/0000-0003-3484-399X
Nianyi Chen https://orcid.org/0000-0001-6627-2533
Simeon Bird https://orcid.org/0000-0001-5803-5490
Nadia Zakamska https://orcid.org/0000-0001-6100-6869
Xin Liu https://orcid.org/0000-0003-0049-5210
Kaitlin M. Kratter https://orcid.org/0000-0001-5253-1338

## References

Amaro-Seoane, P., Andrews, J., Arca Sedda, M., et al. 2022, arXiv:2203.06016
Arzoumanian, Z., Baker, P. T., Blumer, H., et al. 2020, ApJL, 905, L34
Barrows, R. S., Comerford, J. M., Greene, J. E., & Pooley, D. 2016, ApJ, 829, 37
Begelman, M. C., Blandford, R. D., & Rees, M. J. 1980, Natur, 287, 307
Bird, S., Ni, Y., Di Matteo, T., et al. 2022, MNRAS, 512, 3703
Blecha, L., Sijacki, D., Kelley, L. Z., et al. 2016, MNRAS, 456, 961
Bortolas, E., Capelo, P. R., Zana, T., et al. 2020, MNRAS, 498, 3601
Callegari, S., Kazantzidis, S., Mayer, L., et al. 2011, ApJ, 729, 85
Callegari, S., Mayer, L., Kazantzidis, S., et al. 2009, ApJL, 696, L89
Capelo, P. R., Dotti, M., Volonteri, M., et al. 2017, MNRAS, 469, 4437
Chen, N., Di Matteo, T., Ni, Y., et al. 2022b, MNRAS, submitted (arXiv:2208.04970)
Chen, N., Ni, Y., Holgado, A. M., et al. 2022c, MNRAS, 514, 2220
Chen, N., Ni, Y., Tremmel, M., et al. 2022a, MNRAS, 510, 531
Chen, Y., Yu, Q., & Lu, Y. 2020, ApJ, 897, 86

Chen, Y.-C., Hwang, H.-C., Shen, Y., et al. 2022d, ApJ, 925, 162
Civano, F., Elvis, M., Lanzuisi, G., et al. 2010, ApJ, 717, 209
Comerford, J. M., Griffith, R. L., Gerke, B. F., et al. 2009, ApJL, 702, L82
De Rosa, A., Vignali, C., Bogdanović, T., et al. 2019, NewAR, 86, 101525
Djorgovski, S. 1991, in ASP Conf. Ser., 21, The Space Distribution of Quasars, ed. D. Crampton (San Francisco, CA: ASP), 349
Dubois, Y., Pichon, C., Welker, C., et al. 2014, MNRAS, 444, 1453
Duncan, K., Conselice, C. J., Mundy, C., et al. 2019, ApJ, 876, 110
Eftekharzadeh, S., Myers, A. D., Hennawi, J. F., et al. 2017, MNRAS, 468, 77
El-Badry, K., & Rix, H.-W. 2018, MNRAS, 480, 4884
El-Badry, K., Rix, H.-W., Tian, H., Duchene, G., & Moe, M. 2019, MNRAS, 489, 5822
Ellison, S. L., Patton, D. R., Mendel, J. T., & Scudder, J. M. 2011, MNRAS, 418, 2043
Fabricius, C., Luri, X., Arenou, F., et al. 2021, A&A, 649, A5
Feng, Y., Bird, S., Anderson, L., Font-Ribera, A., & Pedersen, C. 2018, MP-Gadget/MP-Gadget: A tag for getting a DOI, Zenodo, doi:10.5281/zenodo.1451799
Gaia Collaboration, Vallenari, A., Brown, A. G. A., et al. 2022, arXiv:2208.00211
Goulding, A. D., Pardo, K., Greene, J. E., et al. 2019, ApJL, 879, L21
Hennawi, J. F., Myers, A. D., Shen, Y., et al. 2010, ApJ, 719, 1672
Hennawi, J. F., Strauss, M. A., Oguri, M., et al. 2006, AJ, 131, 1
Hirschmann, M., Dolag, K., Saro, A., et al. 2014, MNRAS, 442, 2304
Hu, W., Barkana, R., & Gruzinov, A. 2000, PhRvL, 85, 1158
Hui, L., Ostriker, J. P., Tremaine, S., & Witten, E. 2017, PhRvD, 95, 043541
Hwang, H.-C., El-Badry, K., Rix, H.-W., et al. 2022a, ApJL, 933, L32
Hwang, H.-C., Shen, Y., Zakamska, N., & Liu, X. 2020, ApJ, 888, 73
Hwang, H.-C., Ting, Y.-S., & Zakamska, N. L. 2022b, MNRAS, 512, 3383
Inada, N., Oguri, M., Shin, M.-S., et al. 2012, AJ, 143, 119
Kayo, I., & Oguri, M. 2012, MNRAS, 424, 1363
Kelley, L. Z., Blecha, L., & Hernquist, L. 2017, MNRAS, 464, 3131
Khan, F. M., Holley-Bockelmann, K., Berczik, P., & Just, A. 2013, ApJ, 773, 100
Kochanek, C. S., Falco, E. E., & Muñoz, J. A. 1999, ApJ, 510, 590
Komossa, S., Burwitz, V., Hasinger, G., et al. 2003, ApJL, 582, L15
Koss, M., Mushotzky, R., Treister, E., et al. 2012, ApJL, 746, L22
Krone-Martins, A., Delchambre, L., Wertz, O., et al. 2018, A&A, 616, L11
Lemon, C., Anguita, T., Auger, M., et al. 2022b, MNRAS, in press
Lemon, C., Millon, M., Sluse, D., et al. 2022a, A&A, 657, A113
Lemon, C. A., Auger, M. W., & McMahon, R. G. 2019, MNRAS, 483, 4242
Lemon, C. A., Auger, M. W., McMahon, R. G., & Koposov, S. E. 2017, MNRAS, 472, 5023
Lemon, C. A., Auger, M. W., McMahon, R. G., & Ostrovski, F. 2018, MNRAS, 479, 5060
Liu, X., Greene, J. E., Shen, Y., & Strauss, M. A. 2010, ApJL, 715, L30
Liu, X., Shen, Y., & Strauss, M. A. 2012, ApJ, 745, 94
Liu, X., Shen, Y., Strauss, M. A., & Hao, L. 2011, ApJ, 737, 101
Lyke, B. W., Higley, A. N., McLane, J. N., et al. 2020, ApJS, 250, 8
Madau, P., & Dickinson, M. 2014, ARA&A, 52, 415
Makarov, V. V., & Secrest, N. J. 2022, ApJ, 933, 28
Mannucci, F., Pancino, E., Belfiore, F., et al. 2022, NatAs, 6, 1185
Mason, B. D., Wycoff, G. L., Hartkopf, W. I., Douglass, G. G., & Worley, C. E. 2001, AJ, 122, 3466
McWilliams, S. T., Ostriker, J. P., & Pretorius, F. 2014, ApJ, 789, 156
Merritt, D. 2013, Dynamics and Evolution of Galactic Nuclei, Princeton Series in Astrophysics (Princeton, NJ: Princeton Univ. Press)
Milosavljević, M., & Merritt, D. 2001, ApJ, 563, 34
More, A., Oguri, M., Kayo, I., et al. 2016, MNRAS, 456, 1595
Myers, A. D., Palanque-Delabrouille, N., Prakash, A., et al. 2015, ApJS, 221, 27
Myers, A. D., Richards, G. T., Brunner, R. J., et al. 2008, ApJ, 678, 635
Ni, Y., Di Matteo, T., Bird, S., et al. 2022, MNRAS, 513, 670
Oguri, M., Inada, N., Clocchiatti, A., et al. 2008, AJ, 135, 520
Oguri, M., & Marshall, P. J. 2010, MNRAS, 405, 2579
Pfister, H., Volonteri, M., Dubois, Y., Dotti, M., & Colpi, M. 2019, MNRAS, 486, 101
Richards, G. T., Fan, X., Newberg, H. J., et al. 2002, AJ, 123, 2945
Richards, G. T., Strauss, M. A., Fan, X., et al. 2006, AJ, 131, 2766
Riello, M., De Angeli, F., Evans, D. W., et al. 2021, A&A, 649, A3
Rochais, T., Singh, V., Chick, W., et al. 2017, MNRAS, 464, 553
Rosas-Guevara, Y. M., Bower, R. G., McAlpine, S., Bonoli, S., & Tissera, P. B. 2019, MNRAS, 483, 2712
Ross, N. P., Myers, A. D., Sheldon, E. S., et al. 2012, ApJS, 199, 3
Scaramella, R., Amiaux, J., Mellier, Y., et al. 2022, A&A, 662, A112
Shen, Y. 2016, ApJ, 817, 55
Shen, Y., Chen, Y.-C., Hwang, H.-C., et al. 2021, NatAs, 5, 569
Shen, Y., Hwang, H.-C., Zakamska, N., & Liu, X. 2019, ApJL, 885, L4
Shen, Y., Richards, G. T., Strauss, M. A., et al. 2011, ApJS, 194, 45
Silverman, J. D., Tang, S., Lee, K.-G., et al. 2020, ApJ, 899, 154
Spergel, D., Gehrels, N., Baltay, C., et al. 2015, arXiv:1503.03757
Steinborn, L. K., Dolag, K., Comerford, J. M., et al. 2016, MNRAS, 458, 1013
Stemo, A., Comerford, J. M., Barrows, R. S., et al. 2021, ApJ, 923, 36
Tamburello, V., Capelo, P. R., Mayer, L., Bellovary, J. M., & Wadsley, J. W. 2017, MNRAS, 464, 2952
Tamfal, T., Capelo, P. R., Kazantzidis, S., et al. 2018, ApJL, 864, L19
Tremmel, M., Governato, F., Volonteri, M., Quinn, T. R., & Pontzen, A. 2018, MNRAS, 475, 4967
Van Wassenhove, S., Capelo, P. R., Volonteri, M., et al. 2014, MNRAS, 439, 474
Venemans, B. P., Walter, F., Neeleman, M., et al. 2020, ApJ, 904, 130
Volonteri, M., Pfister, H., Beckmann, R., et al. 2022, MNRAS, 514, 640
Xiao, H., Shen, X., Hopkins, P. F., & Zurek, K. M. 2021, JCAP, 2021, 039
Yu, Q. 2002, MNRAS, 331, 935
Yue, M., Fan, X., Yang, J., & Wang, F. 2021, ApJL, 921, L27
Zhan, H. 2021, ChSBu, 66, 1290